# Bayesian Updating for Reduction of Soil Parameter Uncertainty Using Strain Data From Axially Loaded Piles

Greg Kurzepa

Pembroke College

gsk35

June 2, 2025

**Abstract**

Geotechnical uncertainty is a major challenge in construction, including in pile design. Bayesian updating is a framework that promises to address this problem by treating variables as inherently uncertain. It allows multiple sources of data to update one central estimate of soil parameters, while explicitly accounting for uncertainties. Leaner design enabled by reduced uncertainty and the more explicit understanding of risk presented by Bayesian thinking has the potential reduce money, time and material demands of underground construction, as well as reducing its environmental footprint.

In this project Bayesian updating is used to reduce uncertainty on soil parameters around an axially loaded pile. Two deterministic soil-pile models are implemented. Noisy observed data was generated using one of the models by applying gaussian noise to represent aleatoric uncertainties. The observed data was used as evidence to update priors on soil parameters,

and the updated distributions shown and analysed. It was shown that, when applied with care, Bayesian updating is an effective tool in the synthetic scenario presented to learn from pile axial load data by reducing uncertainty of soil parameters.

# Contents

# 1 Introduction

Uncertainty and risk are inherent and dominant in geotechnical engineering and design ((9)), especially regarding variability in soil engineering data where coefficients of variation can exceed 30% ((3)). To address this variability, geotechnical designers have traditionally resorted to conservative design. Conservative design demands more money, time, material and causes more environmental harm than if better knowledge was available and applied to the problem.

Bayesian updating is being increasing applied to geotechnical engineering as a powerful tool to reduce geotechnical uncertainty, and hence reduce overdesign, by learning from data. The Bayesian approach to geotechnical engineering treats data and soil parameters as inherently uncertain, in the form of probability distributions. This enables better understanding of risk compared with traditional practices like Eurocode reduction factors or probability of failure analysis. Data such as ground measurements or strain gauge measurements from piles can be used to update the soil parameter distributions. The stronger the evidence relative to the prior knowledge of the soil parameters, the more the update reduces the uncertainty on the soil parameter distributions. Any data can be used to update the soil parameters as long as the data and the soil parameters can be linked via a mathematical model. New sources of data can progressively update the parameters as they become available ((13)).

Updated soil parameters as discussed in this report have uses in various aspects of design. They could be used to non-destructively extrapolate the ultimate strength of a pile in soil. They can be used to within an observational method like (26), or contribute to 3D BIM maps of soil parameter distributions ((11)). One can envision a BIM platform that incorporates many sources of data around a construction site or a larger area to update geographical models of ground conditions live, maximising certainty about the ground conditions and so enabling leaner design.

In this report, soil parameters surrounding an axially loaded pile are updated using a synthetic observed strain profile of the pile. This synthetic data might represent observations from a static pile load test, or from long-term tracking of the deep foundation behaviour of a building like in

(Babanagar). Updating is tested using two different soil-pile models. The prior and updated soil parameter distributions are compared. The aim of the work is to show that Bayesian updating, by embracing uncertainty instead of avoiding it, is an effective tool for understanding soil behaviour more accurately than the traditional deterministic treatment. The second aim is to demonstrate the importance of model choice and model error in achieving accurate results.

# 2 Literature Review

## 2.1 Uncertainty in Geotechnical Engineering

Geotechnical uncertainty is a major challenge in construction, including pile design ((22)). It is often the cause of delays, cost overruns and failures ((20)). Current geotechnical models are usually biased and imprecise due to the uncertainties involved ((17)), (11)). Soil engineering data is highly uncertain: noise in soil measurements can have a coefficient of variation (standard deviation divided by mean) of 30% or more ((3)). Measurement error can account for 75% of total soil parameter variance ((10)).

The preferred tools for geotechnical engineers to deal with uncertainty are deterministic, including overdesign, safety factors and the observational method ((9)). Experts are systematically confident when reporting uncertainty ((3)), so a rigorous probabilistic approach to account for uncertainty is needed. Probabilistic analysis and design has seen little uptake, partly because it systematically overpredicts probability of failure ((10), (3)). This is due to a past lack of distinction between epistemic and aleatoric uncertainties in modelling ((25)).

Epistemic uncertainty reflects incomplete knowledge about the system being studied, while aleatoric uncertainty reflects uncertainty intrinsic to the system that the model deems inaccessible. For example, lack of knowledge about a soil parameter in a soil may be epistemic, while measurement error that cannot be reduced is aleatoric. (3) says that fundamentally, all uncertainty is epistemic, and aleatoric uncertainties are simply modelling assumptions that some

information is inaccessible.

A probabilistic approach to dealing with uncertainty can provide a better understanding of risk ((10)), allowing for leaner design. A successful approach will require explicit consideration of the various uncertainties.

## 2.2 Observational Method

The preferred way for engineers to learn from data, improve on conservative design and better deal with uncertainty has been the observational method, which is closely related to concepts of Bayesian learning ((9)). Difficulties in assessing the most probable design parameters from back analysis has limited the use of the observational method ((7)). The Tottenham Court Road Station excavation for Crossrail in London ((26)) successfully used the observational method to reduce material use and shorten the construction schedule. The soil parameters surrounding the excavation were back-analysed and tracked during the excavation of the station box, which provided more accurate information about the soil. This updated information allowed the final wall brace to be omitted. The observational method, by putting off some design decisions to the construction stage, has limitations. The engineer must have access to the decision maker, and the decision maker might be constrained by regulators and the public to provide certainty about a project from the outset ((9)).

## 2.3 Bayesian Updating

Bayesian inference (or Bayesian updating) is a more fundamental approach to learning from data. Bayesian thinking embeds the idea of epistemic uncertainty into the uncertain parameters themselves by treating variables as inherently uncertain, represented by probability distributions.

The uncertain parameter distributions can be updated by evidence from data, which may itself be

uncertain. The "prior" parameter distribution is updated by the "likelihood" or "evidence", which expresses the relationship between the uncertain parameter and the data evidence, to produce the updated "posterior" distribution. In geotechnical applications where soil parameters are to be updated, the evidence is in the form of a physical model linking the data to the soil parameters. The uncertain parameter distribution can be updated many times by several sources of data: (3) quoted Lindley, "today's posterior is tomorrow's prior".

When there is little available data, as is usually the case in geotechnical engineering, the prior has a significant contribution to the posterior. The first prior is inherently subjective, and a matter of judgement for the practiotioner ((3)). Often, priors on soil parameters are interpreted from values in the literature or past tests in the same soil.

Care must be taken when applying Bayesian updating; even experts exhibit systematic errors when reasoning about probabilities ((3)). For example, in small-sample datasets diffuse (flat) priors, which are intended to reflect a "no prior knowledge" assumption, should be avoided. Prior and posterior predictive checks, which feed the prior and updated parameter distributions forward through the evidence model, are important to evaluate the update ((24)).

Practical Bayesian updating is almost always carried out using Markov Chain Monte Carlo, a sampling technique. This requires thousands or even tens of thousands of evaluations of the physical model. Thus, advanced techniques like FEM optimised for accuracy are not suitable for updating. Simpler models must be developed at minimum expense of accuracy. For example, (8) updated a spatial profile of soil parameters in a pile wall system, by fitting a surrogate model using Gaussian Processes.

## 2.4 Applications in Geotechnical Engineering

Many research papers have applied Bayesian updating to geotechnical engineering. (13) provide many examples of applications of Bayesian theory to the field, including in embankments, tunnelling, soil tests and piles. Recently, the more popular approach has been to update soil pa-

rameters rather than updating safety factors. (8) references examples of soil parameter updating. (5) used Bayesian updating to reduce uncertainty in soil parameters around a dynamically driven pile.

Most applications of Bayesian updating to axially loaded piles, such as during pile load tests, have been to update resistance or safety factors (such as (16)). This limits the usefulness of the pile load test to design of piles. Since pile load tests are expensive, it would be desirable to learn more from them. In this research the alternative approach is taken, using strain profiles from an axially loaded pile to update soil parameters surrounding the pile. This is more general, providing an understanding of the soil itself. This allows for very broad applications, and could contribute to work in BIM applications such as (Babanagar) or geographic soil distribution models (discussed by (11)).

The model is an implementation t-z and q-z analysis of soil stiffness, a widely used approach in physical modelling of piles ((4)).

# 3 Methods

## 3.1 Problem Definition: Back-Analysis of Soil Parameters from Pile Strain Gauge Data

In this project, synthetic pile strain-gauge data in the form of the profile of pile strain with depth is used as evidence to update prior beliefs on the soil parameters. The prior and posterior distributions are then compared with the ground truth soil parameters.

The deterministic function that links the soil parameters $\boldsymbol{\theta}$ to the resulting unseen pile strains $\boldsymbol{\varepsilon} = f(\boldsymbol{\theta})$ is the soil-pile model, referred to here as $f$. In this report an encompassing error term $\eta$ that includes all aleatoric errors such as measurement noise and spatial soil variation is assumed. The error term is taken to be white noise with mean 0 and variance $\sigma_\eta^2$. In this way, the observed

strains are given by eq. 1. The likelihood of a specific strain distribution $\varepsilon_\eta$ being observed from the unseen strain distribution $f(\boldsymbol{\theta})$ is given by a gaussian distribution as in eq. 2.

$$\varepsilon_\eta = f(\boldsymbol{\theta}) + \eta \tag{1}$$

$$p(\varepsilon_\eta|\boldsymbol{\theta}) \sim \mathcal{N}(\varepsilon_\eta; f(\boldsymbol{\theta}), \sigma_\eta^2) \tag{2}$$

A noisy set of synthetic observations is generated using the non-linear model to act as the evidence. This means the linear-elastic model will have some model error with respect to these observations, while the non-linear model will have none. These noisy observations are shown in fig. 1.

The noisy observations were generated as follows. There are two soil layers: loose sand to 12.5m depth and dense sand to 30m depth, which is the pile base. The parameters specified in table 1 and table 2 were used to deterministically generate the ground truth strain profile using the non-linear model. The soil parameters within a layer are assumed uniform. Gaussian white noise with standard deviation of 20 microstrains was added to the profile to generate the observations. This standard deviation is typical for measurement error for fiber optic strain gauges ((14)), but is an underestimate of the total uncertainty since other aleatoric uncertainties that might be included in the noise, like spatial soil variability, have not been taken account of.

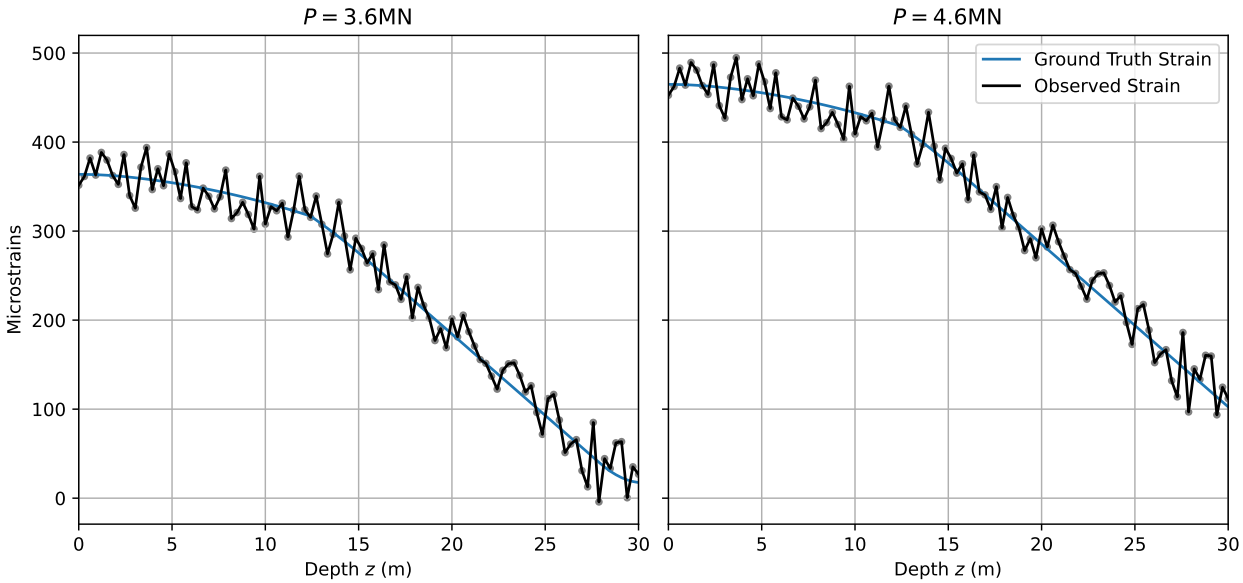


Figure 1: The synthetic ground truth and noisy strain observations used as the evidence for inference. Left: Compressive axial load 3.6MN; Right: 4.6MN.

| | Clay or Sand | Base Depth (m) | Dry Unit Weight $\gamma_d$ (kN/m) | Void Ratio $e$ | Shaft Friction Factor $\beta$ | Shaft Friction Limit $\tau_{\text{cap}}$ (kPa) | End Bearing Factor $N_q$ | End Pressure Limit $q_{\text{cap}}$ (MPa) |
|---|---|---|---|---|---|---|---|---|
| **Layer 1** | Loose Sand | 12.5 | 15 | 0.689 | 0.2675 | 47.8 | 8 | - |
| **Layer 2** | Dense Sand | 30.0 | 17 | 0.441 | 0.575 | 96 | 40 | 10 |

Table 1: Ground Truth Soil Parameters for Nonlinear Model

| $P$ (MN) | Discretisation Element Count $N$ | Pile Modulus $E_P$ (GPa) | Pile Diameter $D$ (m) | Pile Length $L$ (m) | Water Table Depth $z_w$ (m) |
|---|---|---|---|---|---|
| 3.6, 4.6 | 100 | 35 | 0.6 | 30 | 3 |

Table 2: Other Parameters, Common to Both Models

In a real life scenario, most or all of the soil parameters would be uncertain. In this report, the ground truth soil parameters are known so any group of them can be hidden from the model and given priors to be updated, while the rest are certain.

Inference experiments for the linear-elastic model were carried with uniform priors as in table 3 and two different loads as in table 2.

Inference experiments for the nonlinear model were carried out as follows. The variables chosen for inference were those that were shown to have a significant impact on the strain profile, as in fig. 6. The means and standard deviations of the informative priors in table 4 were chosen to roughly encapsulate the possible range of values for the layer's soil type (e.g. loose sand or dense sand), which is assumed to be known by the practitioner in advance of inference. The values of the means and standard deviations were interpreted from the API specification.

First, only the dry unit weight was inferred for both layers. To compare the effect of an informative and non-informative (diffuse) prior, this single-variable inference was carried out twice, once with the informative priors and once with non-informative uniform priors. The non-inferred variables are taken to be the ground truth values in table 4. Second, the four most important soil parameters (see Sensitivity Analysis in Results) were inferred as in table 4, to assess the impact on the posterior when more parameters are inferred.

| | Shaft Winkler Modulus $E_{s,1}$ and $E_{s,2}$ (MPa) | End Bearing Stiffness $K_b$ (MN/m) |
|---|---|---|
| **Distribution** | Uniform | Uniform |
| **Value (Both Layers)** | 0.1 to 1000 | 0.1 to 1000 |

Table 3: Priors on Soil Parameters for Linear-Elastic Model. The priors are all independent (uncorrelated).

| | Dry Unit Weight $\gamma_d$ (kN/m) Informative | Dry Unit Weight $\gamma_d$ (kN/m) Uninformative | Void Ratio $e$ | Shaft Friction Factor $\beta$ | Shaft Friction Limit $\tau_{\text{cap}}$(kPa) |
|---|---|---|---|---|---|
| **Distribution** | Lognormal | Uniform | Truncated Normal | Lognormal | Lognormal |
| **Top layer** | $\mu$ = 14.5<br>$\sigma$ = 3 | lower=9<br>upper=30 | $\mu$ = 0.8<br>$\sigma$ = 0.2<br>lower=0.01, upper= 1 | $\mu$ = 0.214<br>$\sigma$ = 0.08 | $\mu$ = 47.8<br>$\sigma$ = 20 |
| **Bottom Layer** | $\mu$ = 18<br>$\sigma$ = 3 | lower=9<br>upper=30 | $\mu$ = 0.45, $\sigma$ = 0.2<br>lower=0.01, upper= 1 | $\mu$ = 0.46<br>$\sigma$ = 0.08 | $\mu$ = 96<br>$\sigma$ = 20 |

Table 4: Priors on Soil Parameters for the Nonlinear Model. The priors are all independent (uncorrelated).

## 3.2 Deterministic Soil-Pile Model

### 3.2.1 Model Definition and Assumptions

The deterministic soil-pile interaction model that maps the soil parameters to the displacements $f := \boldsymbol{\theta} \mapsto u(z)$ is defined here, as presented in (21). The model is stiffness-based. The pile is modeled as a 1-dimensional beam axially loaded by known force $P$. The soil resists by exerting a shear friction on the pile walls $\tau(u(z))$ and an end bearing pressure on the pile base $Q(u(z = L))$. There is no slip between the soil and the pile. The pile stress-strain relationship is expressed with a stress function $\sigma(\varepsilon)$, as in eq. 3. The equilibrium condition shown in fig. 2 is expressed in eq. 4. Combining eq. 3 and eq. 4 yields the differential equation in eq. 5. Note, $A$ and $C$ are the pile cross-sectional area and circumference. $\varepsilon$ is the strain in the pile and soil and $F$ is the axial force in the pile. Strains, stresses and forces are compression positive.

$$\begin{aligned} \varepsilon &= -\frac{du}{dz} \\ F &= A\sigma\left(-\frac{du}{dz}\right) \end{aligned} \tag{3}$$

$$-\frac{dF}{dz} = C\tau(z) \tag{4}$$

$$A\frac{d^2u}{dz^2}\sigma\left(\frac{du}{dz}\right) = C\tau(z) \tag{5}$$

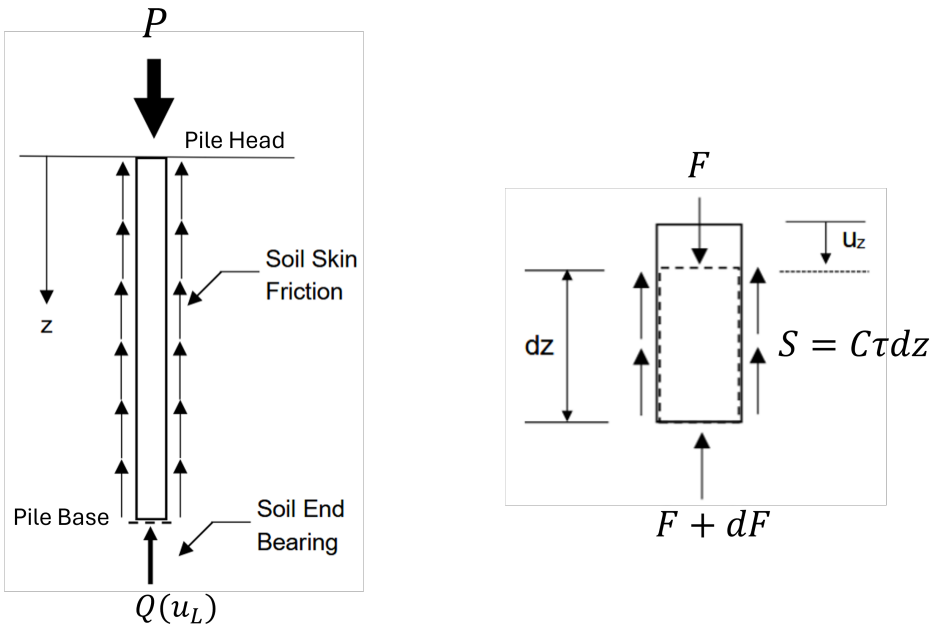


Figure 2: Insert figure caption here

The system is subject to two boundary conditions, expressed in eq. 6. The first is a condition on the strain at the top of the pile, which is set by the known loading. The second is the condition that the end bearing force must bring the pile into equilibrium.

$$\begin{aligned} \varepsilon_0 \equiv \varepsilon(z=0) \equiv -\frac{du}{dz}(z=0) &= \sigma^{-1}\left(\frac{P}{A}\right) \\ F(z=L) \equiv A\sigma\left(-\frac{du}{dz}(z=L)\right) &= Q(u(z=L)) \end{aligned} \tag{6}$$

Two variations on this model that are used in the report are outlined below.

### 3.2.2 Linear-Elastic Soil Case

The pile is given a uniform elastic modulus $E_P$. The soil shear friction and end bearing pressure are expressed using a Winkler Modulus $E_S$ and end bearing stiffness $K_B$ respectively, as in (19).

This leads to the simplifications shown in eq. 7

$$\begin{aligned} \sigma\left(-\frac{du}{dz}\right) &= -E_P\frac{du}{dz} \\ \tau(z) &= E_s u(z) \\ Q &= K_B u(z = L) \end{aligned} \tag{7}$$

The solution to the system can be solved analytically, as shown in eq. 8, where $B$ and $C$ are set by boundary conditions at the head and base of the pile.

$$\begin{aligned} u &= B\exp[\lambda z] + C\exp[-\lambda z] \\ \lambda &= \sqrt{\frac{CE_s}{AE_p}} \end{aligned} \tag{8}$$

The solution can be extended to multiple soil layers with each given its own Winkler Modulus $E_{s,i}$. The solution is treated as piecewise in the domain of each layer; the constants $B$ and $C$ for each layer can be found by enforcing compatibility at layer boundaries as well as the top and bottom boundary conditions. The solution for two soil layers can be found in the Appendix.

The key flaw of this model is that it does not account for loss of strength in the pile and soil at higher loading; it allows for unlimited axial capacity and unlimited settlement.

### 3.2.3 Nonlinear Soil Case

The API (American Petroleum Institute) soil model, taken from (12), improves on the linear-elastic soil model by accounting for loss of soil strength at higher loading. The shear friction and end bearing pressure functions are defined using t-z and Q-z curves, shown in fig. 3, referred to as $\hat{\tau}(u)$ and $\hat{Q}(u)$ respectively.

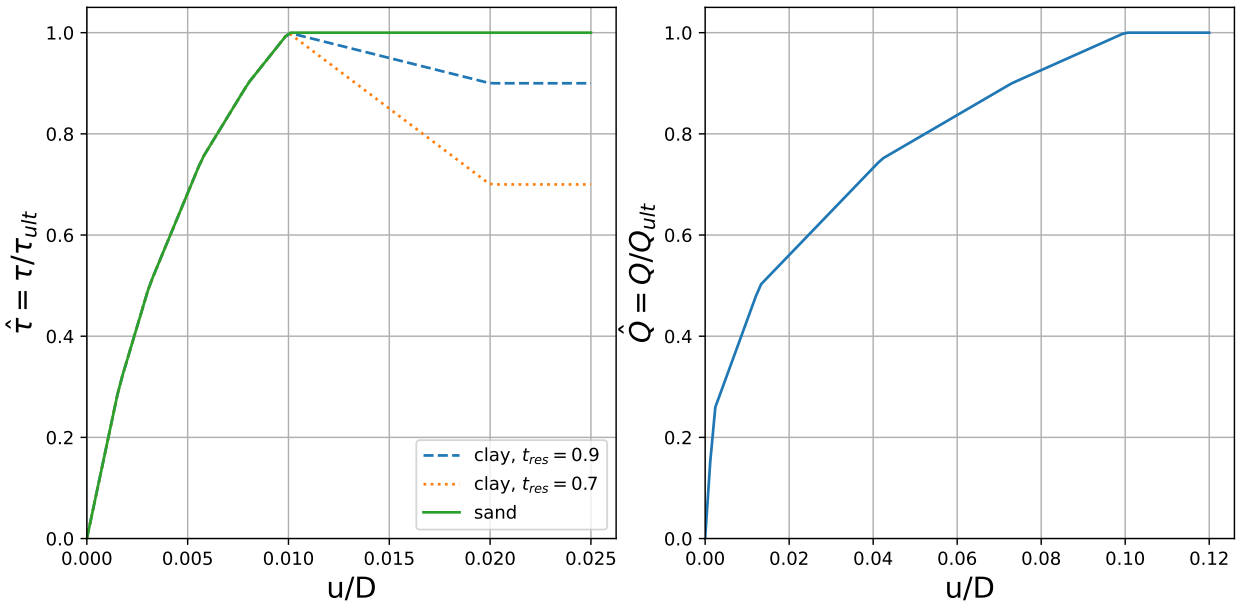


Figure 3: Insert figure caption here

The values of shear and end bearing pressure depend on the of the ultimate shear strength $\tau_{ult}(z)$ and ultimate end bearing strength $Q_{ult}$ of the soil. Additionally, in soils there is a fixed upper limit defined on the shear and end bearing that can be mobilised. The ultimate shear strengths and upper limits are defined in the Appendix.

In this case the differential equation in eq. 5 is nonlinear (due to the nonlinear t-z and Q-z curves) so cannot be solved analytically. Multiple numerical approaches to solving the discretised system were tested and compared for numerical robustness, discussion of which can be found in the Validation section.

## 3.3 Bayesian Updating and MCMC

### 3.3.1 Bayesian Updating

Bayesian updating is a mathematically rigorous framework for working with uncertainties by representing variables (such as soil parameters or ground measurements) with PDFs instead of single values. It allows multiple uncertain sources of information about a target variable or set

of variables to be aggregated into an overall PDF on that variable by ”updating” the knowledge about the variable(s) using inference steps. A single inference step is:

$$p(\boldsymbol{\theta}|x) = \frac{1}{Z} p(\boldsymbol{\theta}) p(x|\boldsymbol{\theta}) \tag{9}$$

Here, $p(\boldsymbol{\theta})$ is the prior on $\boldsymbol{\theta}$, representing the knowledge about the variable before the new data is seen. $p(x|\boldsymbol{\theta})$ is the likelihood, also known as the evidence. It represents the information gained from new data $x$ (for example the strain gauge readings, $x = \varepsilon$). The posterior is on the left, representing the updated knowledge about $\boldsymbol{\theta}$ accounting for both the prior and the evidence. $Z$ is the scaling factor to ensure the posterior is a valid probability distribution. If the forward problem is ($\boldsymbol{\theta} \rightarrow x$), inference solves the inverse problem ($\boldsymbol{\theta} \leftarrow x$).

If more evidence becomes available, the posterior can become the new prior and the updating process can be repeated to further improve the certainty about $\boldsymbol{\theta}$. Many inferences can be carried out, and if desired each inference can link data related to the parameters via a different model (the model is expressed in the likelihood). If the datasets are statistically independent, then $n$ inference steps are expressed as

$$p(\boldsymbol{\theta}|x_1, ...x_n) = \frac{1}{Z} p(\boldsymbol{\theta}) \prod_{i=1}^{n} p(x_i|\boldsymbol{\theta}) \tag{10}$$

The big picture is that several different sources of data can be used to improve knowledge of the soil parameters and bring them as close to a perfect measurement as possible.

In this report, $\boldsymbol{\theta}$ are the soil parameters and $x$ is strain gauge data. One source of data is linked to the soil parameters via one model as a proof of concept. However, it is possible to update the soil parameters many times using various models, as described above.

### 3.3.2 Markov Chain Monte-Carlo

In order to analytically compute the posterior distribution, the scaling term $\frac{1}{Z}$ must be known. For eq. 9, the scaling term is

$$Z = \int p(\boldsymbol{\theta})p(x|\boldsymbol{\theta})d\boldsymbol{\theta} \tag{11}$$

This can only be analytically computed for specific forms of the likelihood and prior densities, notably if both are Gaussian functions.

In the case of the soil-pile system, most parameters that could be inferred (including most soil properties and the measurement error standard deviation) cannot be negative, so a Gaussian prior is inappropriate. In literature these priors are typically defined as truncated Gaussians or, as in this report, Lognormal distributions ((23)). Therefore the scaling factor cannot be analytically computed.

Markov Chain Monte-Carlo (MCMC) is an umbrella of numerical techniques to estimate the posterior by sampling from its distribution, allowing it to be reconstructed. MCMC is ubiquitous in practical Bayesian inference applications. A Markov Chain with stationary distribution matching the posterior is initialised and repeatedly stepped forward to ”draw” from the posterior.

In modern applications, the state-of-the-art MCMC algorithm is No U-Turn Sampling (NUTS), which is based on Hamiltonian Monte Carlo (HMC). In essence, a ”particle” is ”rolled” along the posterior surface, allowing the posterior space to be explored effectively. It requires that both the likelihood and the gradient of the likelilhood be available. It may be possible to implement the gradient (using a shooting method built in JAX and Diffrax for Python) but an implementation was considered too complex this work.

A suitable sampling algorithm when likelihood gradients are not available is Sequential Monte Carlo (SMC), which is used in this report. It explores the posterior space much more effectively than other non-gradient-based MCMC algorithms such as Metropolis-Hastings. The implementation of the SMC algorithm is left to PyMC ((1)), which also offers diagnostic tools to ensure

convergence of the posterior distribution estimate. All inferences were carried out with 2000 draws from the posterior, which was checked to be sufficient for each case.

# 4 Results

### 4.0.1 Validation Against Literature

To validate the output of the nonlinear model, the output axial force profile was compared with an example from literature.

(Poulos) provides reference data for a pile under static axial loading. The soil layers are specified as loose sand down to 12.5m and dense sand down to 30m. The theoretical model used by Poulos was different to the model used in this report but also stiffness-based. The API parameters for the nonlinear model used in this report (presented in section 3.1) were chosen to roughly match the Poulos soil layer categories. Thus, agreement was is expected to be perfect.

The force profiles for two axial head load values are compared in fig. 4. The force profile generated by the API model shows rough agreement with the Poulos theoretical and empirical results.

Pile head and base settlements for loads up to the ultimate axial pile load are compared in fig. 5. The agreement for head settlement is good until loads close to the ultimate load are reached. The agreement for base settlement is extremely poor, suggesting that the API model is unsuitable for predicting pile displacements at depth. It may also point to an error in this report's implementation (further validation would have been enlightening but was not carried out).

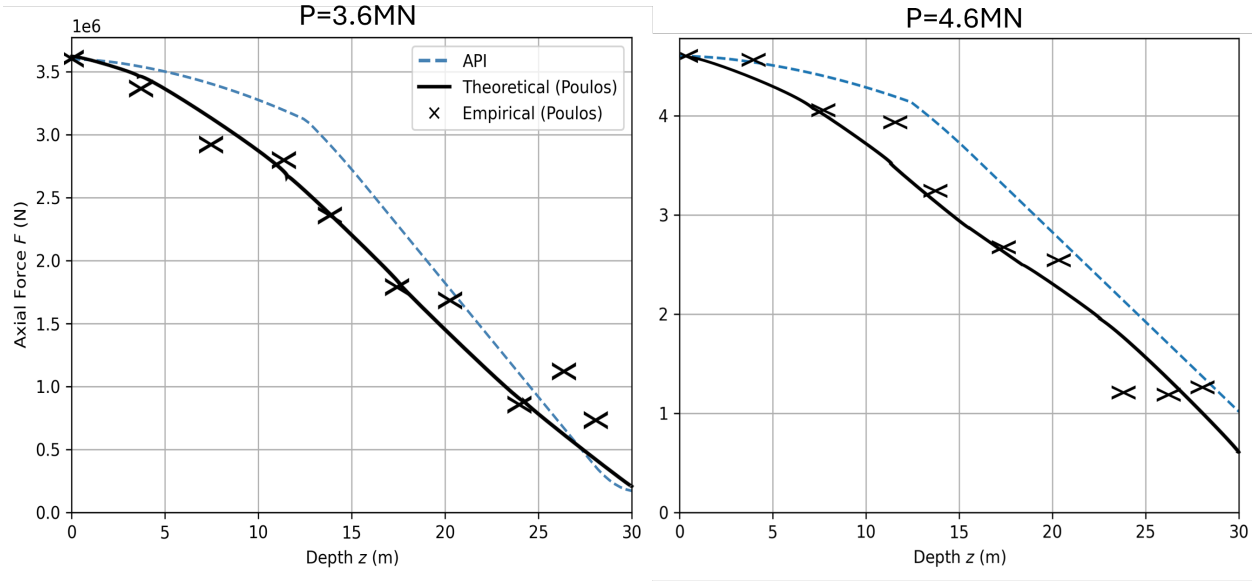


Figure 4: Comparison of non-linear model force profile (dashed) with Poulos 1989 theoretical (line) and empirical (crosses) results for axial load 3.6MN, 4.6MN

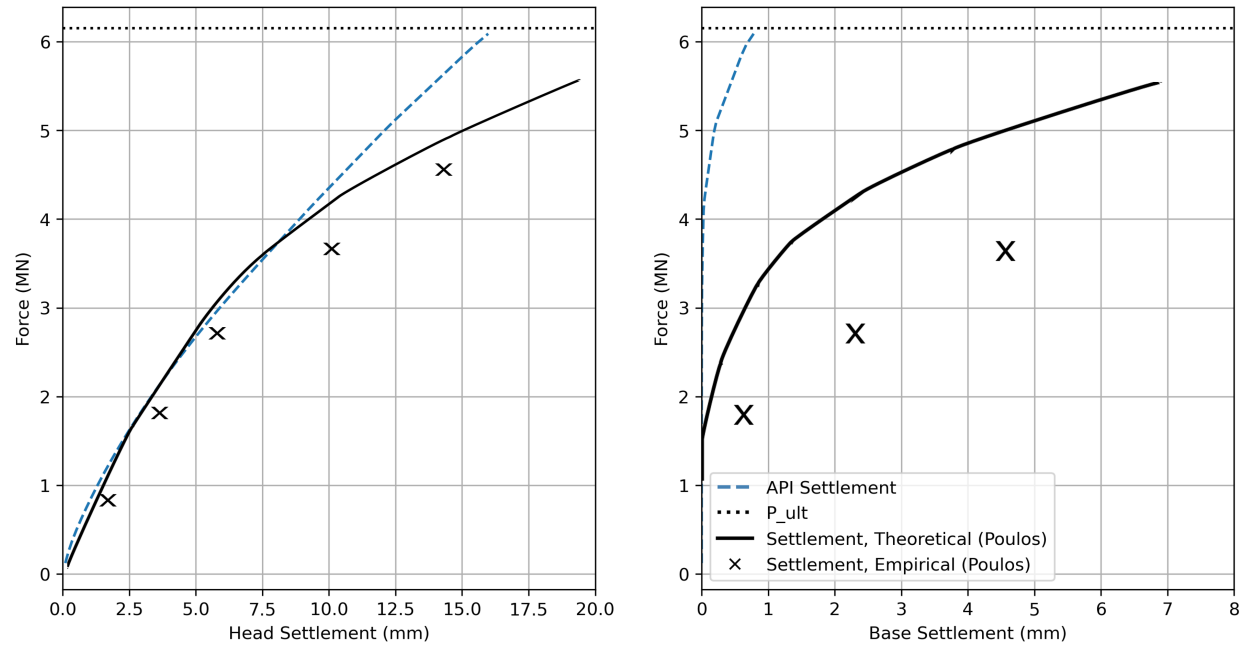


Figure 5: Comparison of head and base settlements as a function of axial load. Dashed: non-linear model. Line: Poulos 1989, theoretical. Crosses: Poulos 1989, empirical.

### 4.0.2 Sensitivity Analysis

The sensitivity of the strain profile to the inferrable parameters in the nonlinear model is shown here.

The sensitivity of the solution when the same parameter is modified in the same way in both layers is shown in fig. 6 for the 3.6MN load case. The four parameters that seem to have a significant impact on the strain were the ones chosen for multi-variable inference.

The sensitivity of the solution to a change in dry unit weight in each layer independently is shown in fig. 7. It is evident that the dry unit weight has a greater impact in the upper soil layer. This is may be because soil weight higher up will increase effective stress over a larger portion of the profile, thus having a greater impact on the soil resistance.

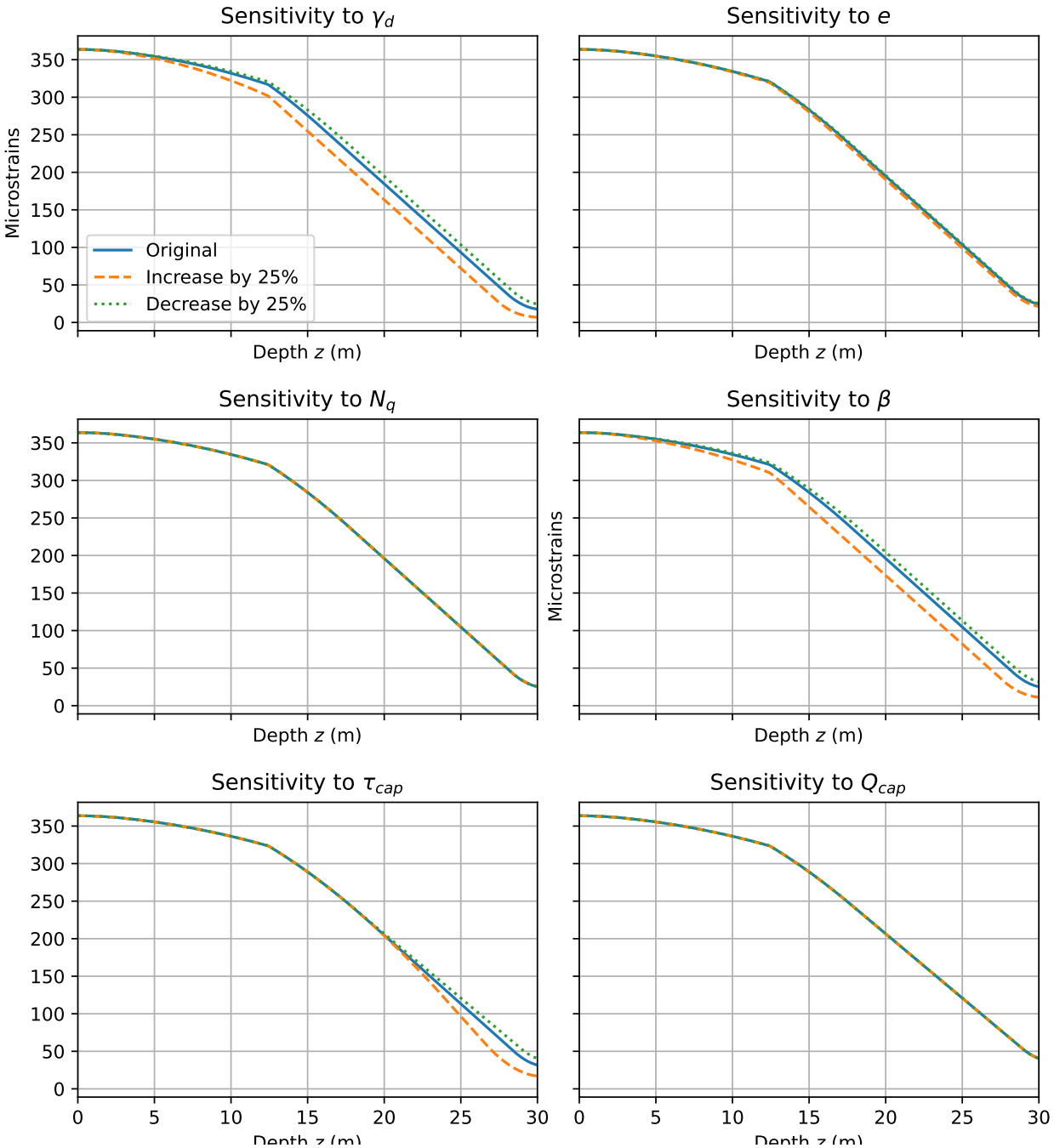


Figure 6: Sensitivity analysis with 3.6MN load for 6 soil parameters. $Q_{cap}$ and $N_q$ likely have a more significant effect when $P$ is closer to $P_{ult}$ (here, $P_{ult} = 6.2MN$).

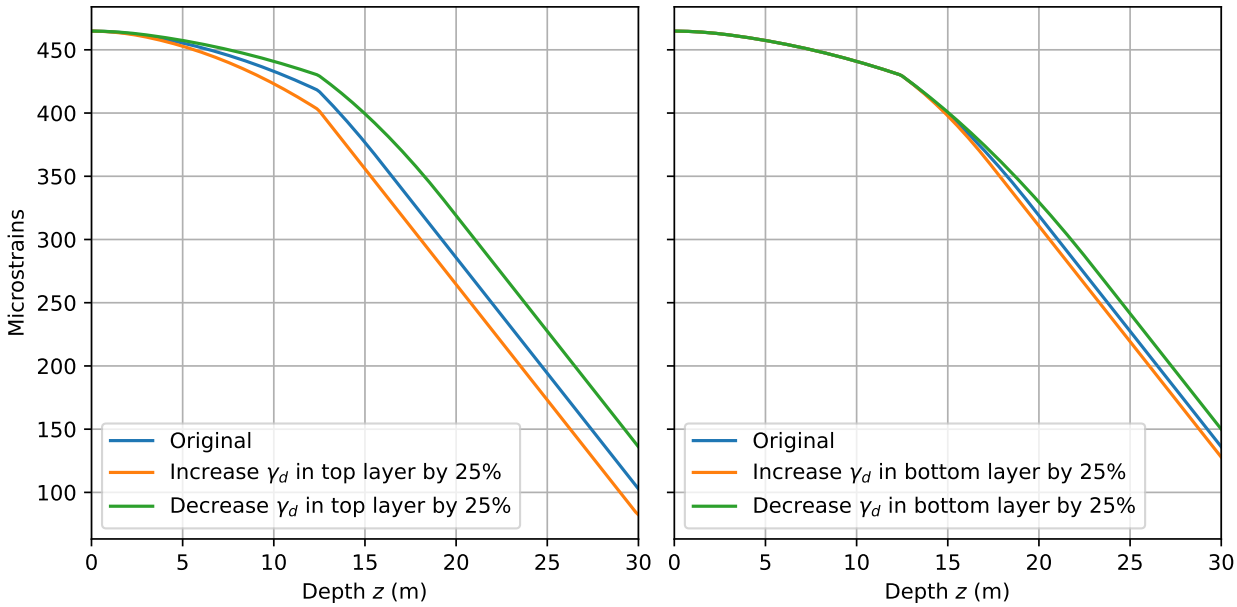


Figure 7: Sensitivity analysis on $\gamma_d$ with 3.6MN load. The upper layer has a larger impact on the strain profile.

## 4.1 Inference

### 4.1.1 Inference With Linear-Elastic Model

fig. 8 shows the posterior distributions of soil parameters with two different load cases. Despite the posteriors suggesting different $E_s$ and $K_b$ values for the two load cases, the ground truth observations and nonlinear API soil parameters that generated them were the same. This exposes the model error in the linear-elastic model: while it parameters can be inferred to match a strain profile, those parameters are not necessarily physically meaningful.

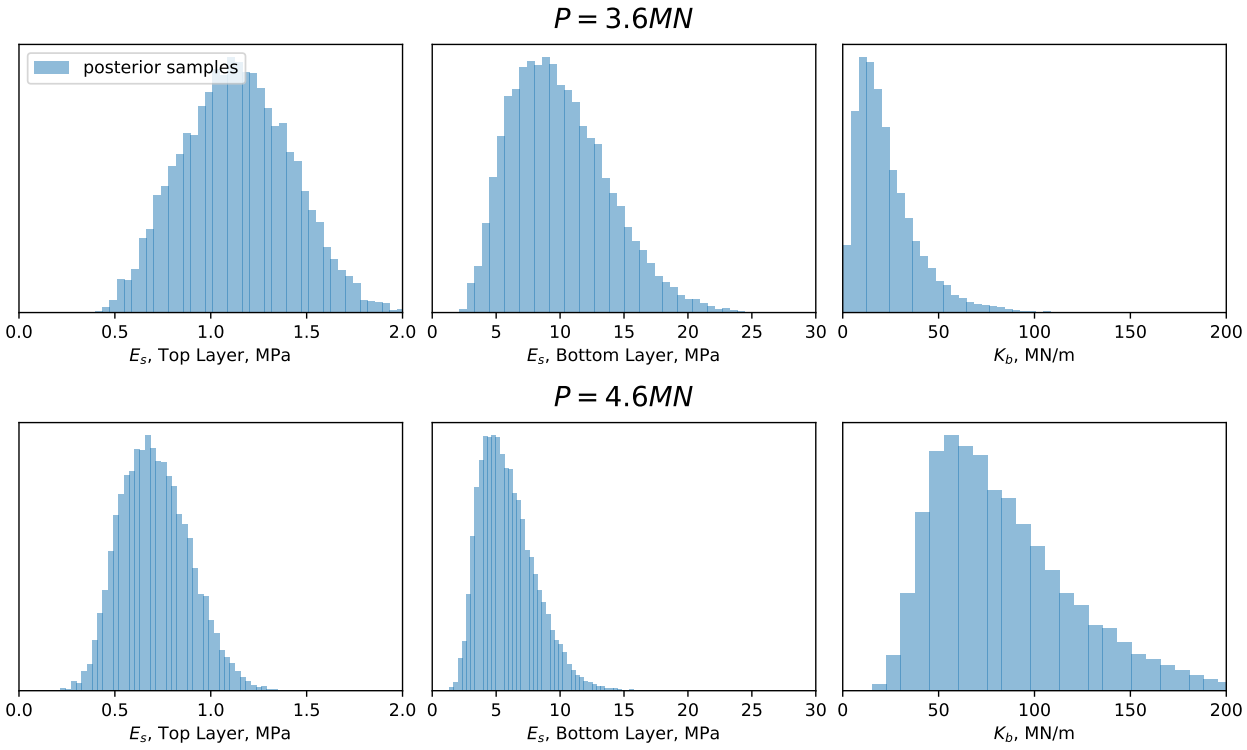


Figure 8:

### 4.1.2 Inference With Non-Linear Model

**Single Parameter Inference** fig. 9 shows prior and posterior soil parameters for the two load cases. Only $\gamma_d$ was inferred for both layers. All other soil parameters were known. For both load cases, the model correctly inferred the same soil parameters. This is because the physical model used in inference here is the same as the data-generating model: there is no model error.

The uncertainty in the top layer decreased drastically, while uncertainty in the bottom soil layer did not improve . This may be because the deterministic strain profile depends much more strongly on the $\gamma_d$ in the top layer than the bottom layer (as in fig. 7. Thus, there is much less information contained in the observed strain profile about $\gamma_d$ in the bottom layer.

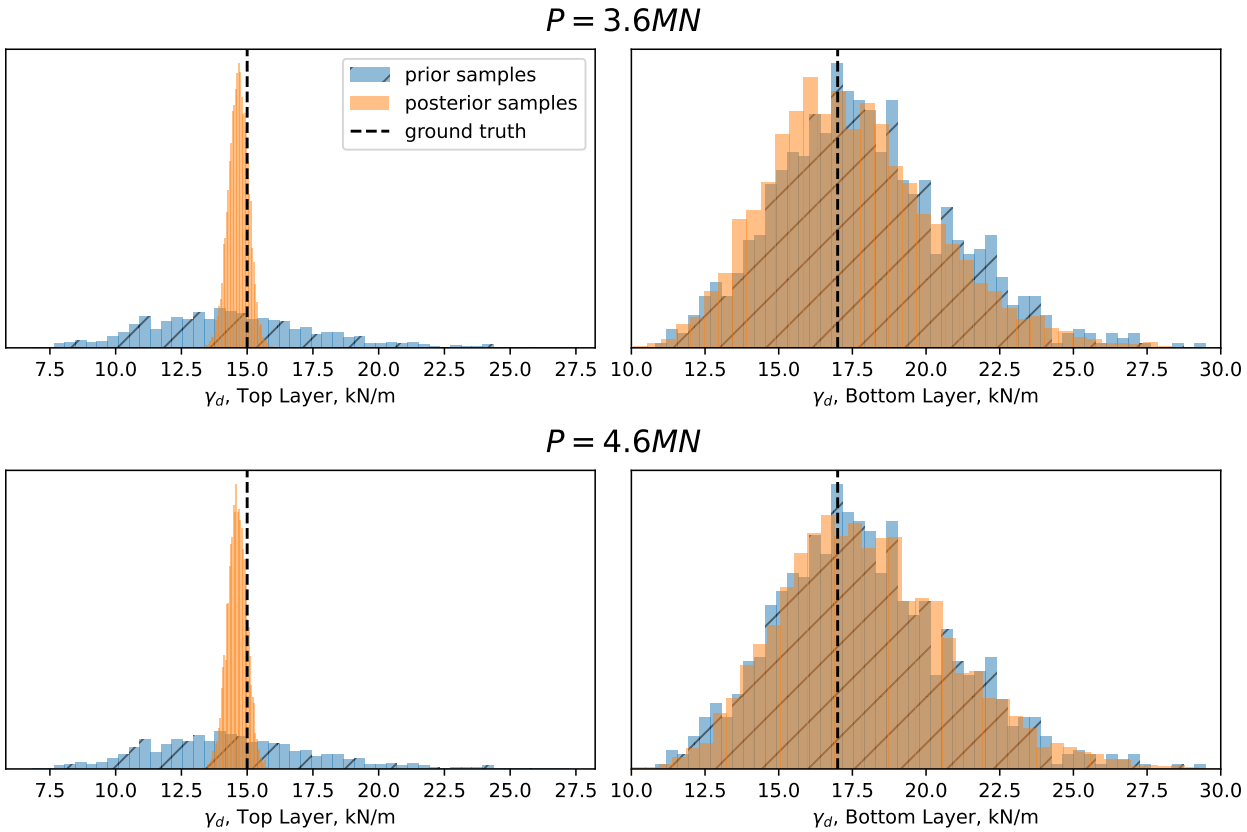


Figure 9:

**Comparison Between Informative and Diffuse Prior** The relative contribution of the prior and likelihood to the posterior depends on the "strength" of each. If the prior probability density is very flat (or uninformative, as it is not confident about the soil parameters) and the likelihood probability density is very narrow, then the likelihood will dominate the posterior, and vice versa.

(15) showed that uninformative priors may lead to inaccurate results with small sample datasets, since in this case both the prior and the likelihood are flat. The likelihood will not be strong enough to overcome the uninformative prior. Any likelihood that contains little information about a specific parameter will lead to poor inference results for that parameter.

Single-variable inference was carried out and for an informative and uninformative prior (priors specificed in table 4). The posteriors are compared in fig. 10. It is evident that the posterior using the uninformative prior is flatter (less certain) than with the informative prior in both layers.

This is because inference did not have access to the domain knowledge that is encoded in the informative prior. The parameter in the bottom layer suffered the most, since the likelihood contains little information about it: the diffuse prior dominates.

This shows that care needs to be taken when specifying priors in inference with small datasets where the initial prior will not be dominated by the data evidence (likelihood). A flat prior such as the uniform distribution here assumes a total lack of knowledge about the soil parameters, is incorrect here since the soil layers are known to be loose and dense sand.

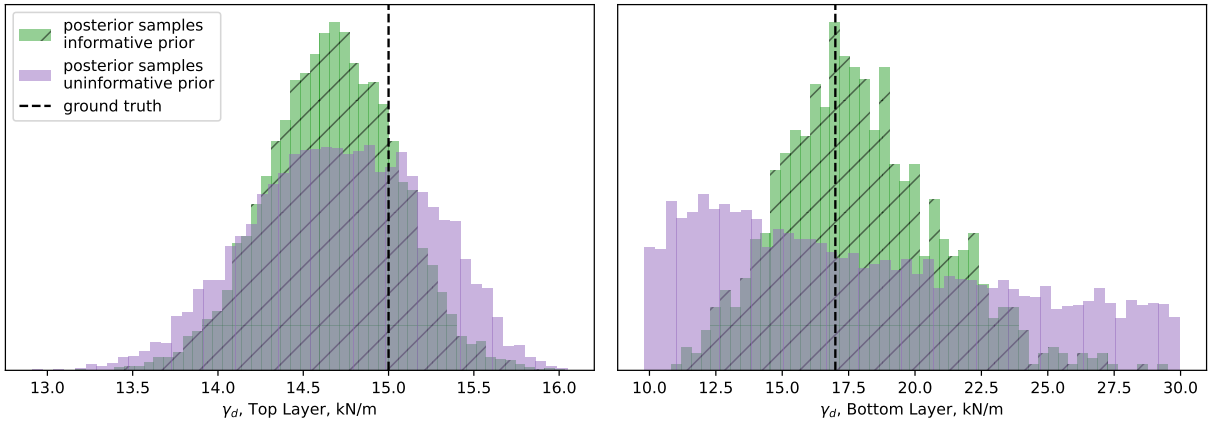


Figure 10: Posterior soil $\gamma_d$ distribution comparison for an informative prior (hatched, green) and an uniformative prior (purple). The uninformative prior

**Multiple Parameter Inference** The priors and posteriors for multi-parameter inference are shown in fig. 11.

The largest decrease in uncertainty was in the shear mobilisation limit $\tau_{cap}$ in the bottom layer. This is explained by the fact that in the bottom layer, $\tau_{ult}$ begins to exceed $\tau_{cap}$ and thus $\tau_{cap}$ begins to have a significant effect on the mobilised shaft friction. The impact of $\tau_{cap}$ on the shaft friction is explained in fig. 17.

The uncertainty on $e$ did not change significantly. This is expected; of the inferred parameters, the strain profile is the least sensitive to $e$ (see fig. 6).

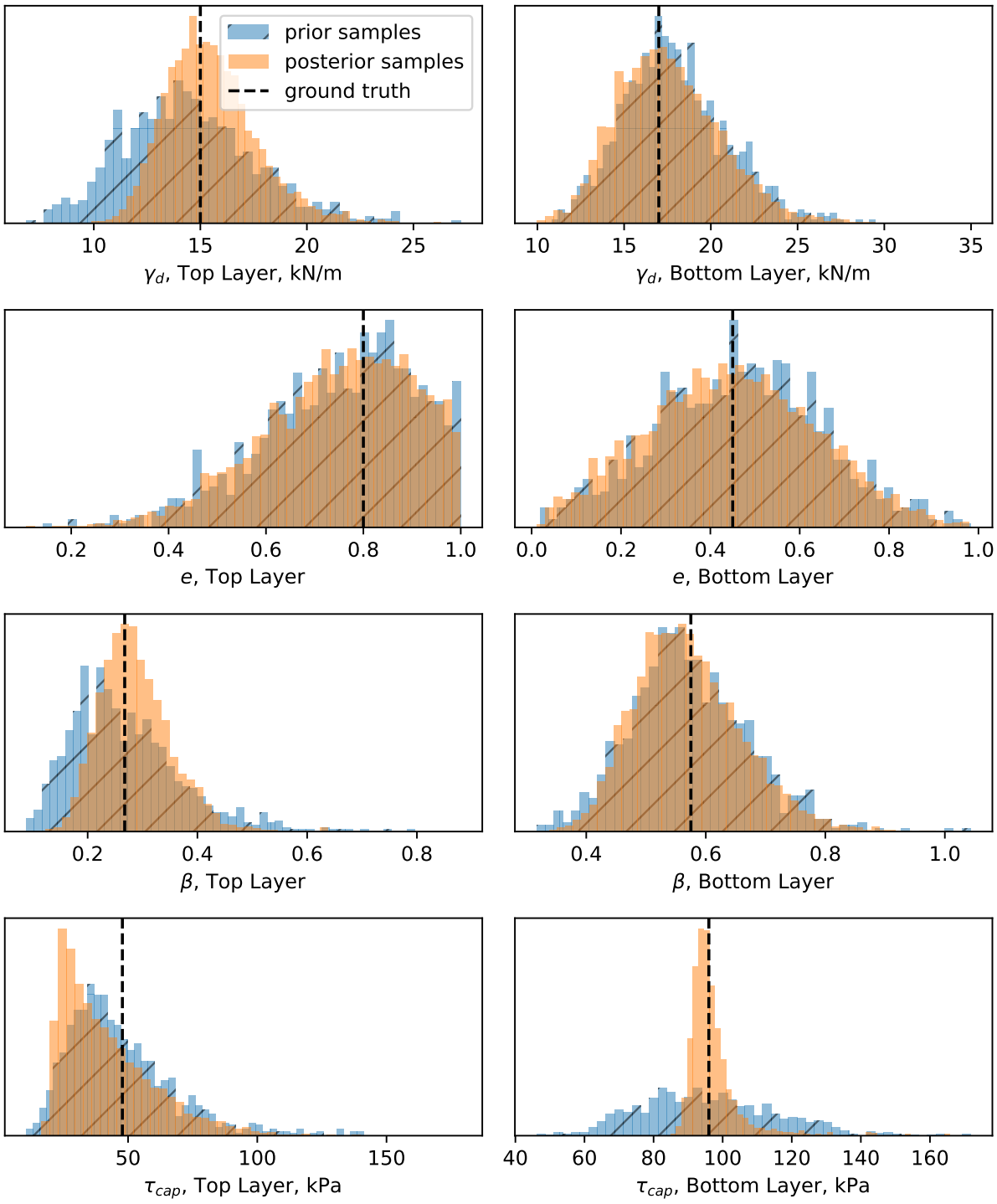
prior samples
posterior samples
ground truth
10
15
20
25
$\gamma_d$, Top Layer, kN/m
10
15
20
25
30
35
$\gamma_d$, Bottom Layer, kN/m
0.2
0.4
0.6
0.8
1.0
$e$, Top Layer
0.0
0.2
0.4
0.6
0.8
1.0
$e$, Bottom Layer
0.2
0.4
0.6
0.8
$\beta$, Top Layer
0.4
0.6
0.8
1.0
$\beta$, Bottom Layer
50
100
150
$\tau_{cap}$, Top Layer, kPa
40
60
80
100
120
140
160
$\tau_{cap}$, Bottom Layer, kPa

Figure 11:

**Impact of Inferring More Parameters** fig. 12 compares the posterior on $\gamma_d$ from the single-parameter inference in fig. 9 and the multi-parameter inference in fig. 11. It is evident that increasing the number of inferred parameters negatively affected the reduction of uncertainty in $\gamma_d$. This is because in the single-parameter experiment, the model had access to perfect knowledge of the three variables that in the multi-parameter experiment were treated as uncertain. The certainty about the other parameters in the single-parameter inference restricted the likely values that $\gamma_d$ could take.

It is incorrect to state that inferring more parameters reduces the "accuracy" of the posterior result. Conversely, accounting for the uncertainty in all parameters that are truly uncertain is essential for an accurate result. If the value of a soil parameter is not known perfectly but it is treated as a known variable in the inference (i.e. it is not given a prior and inferred), any error in the provided value of that parameter will introduce bias into the posterior estimates. The confidence on other uncertain parameters in the model will be inflated. This is shown in fig. 12: the posterior density for $\gamma_d$ is artificially inflated in the single-parameter inference.

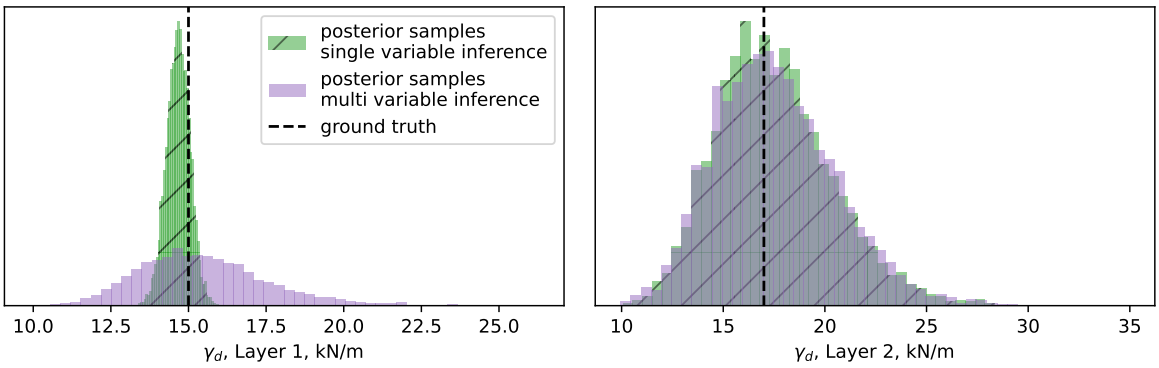


Figure 12:

## 4.2 Discussion, Limitations and Extensions

"All models are wrong" is a common adage in statistics, and applies equally here. In the inference presented in this report the nonlinear API model, used to generate the synthetic observa-

tions, acted as the true representation of reality. In fact, the physical model contains numerous deficiencies that separate if from reality. Important soil effects like interface slip and ground heave or residual stresses due to pile driving were not considered. The pile was treated as a perfectly-elastic material with infinite strength, and was given the same stiffness in tension and compression. These deficiencies restrict the model from being used for application to realistic scenarios and real-world datasets. This is the most direct approach to further development of the work. For example, the effect of soil heave is important in driven piles and piled foundations ((6)) so needs to be accounted for to be applicable, for example, for back analysis to a dataset like (Babanagar), which collected strain data about a pile supporting an excavation. Pile-soil interface slip and residual stresses are other important effects that were not considered but have been shown to be important ((Poulos)).

The safest way to use the prior or inferred soil parameter distributions is to feed them back through the deterministic physical model to generate probability distributions on the pile displacement, strain, and force. If the prior is used, this is called the prior predictive distribution, and if the posterior is used, this is called the posterior predictive distribution. This way, one aspect of model error is mitigated: even if the inferred soil parameters do not have physical meaning, they may still provide good posterior predictive distributions. Applications include testing to enable design of optimised piles that will be driven into the same soil, or non-destructive testing of a pile to extrapolate its ultimate axial capacity.

The inherent model error discussed above means that using the back-analysed soil parameters for applications other than predictions using the same model that inferred them must be done carefully. The real-world accuracy of the deterministic model should be carefully evaluated in the context it will be applied.

The real-world performance of any soil parameter back-analysis scheme is difficult to evaluate, since the ground truth soil parameters are not available. Indeed, these methods look to improve the soil parameter estimates beyond the noisy and highly uncertain measurements available

from direct soil testing.

# 5 Conclusion

Bayesian updating was applied to a 1-dimensional axially loaded pile problem. A linear-elastic physical soil-pile model was implemented using a Winkler modulus for the soil. A nonlinear physical soil-pile using the API specification. Synthetic ground truth and noisy observed data was generated using the nonlinear model. Soil priors were updated and the posterior distributions shown and analysed. It was shown that Bayesian updating is an effective tool to reduce uncertainty in knowledge of soil parameters in the synthetic scenario presented. Potential application to real-world cases was discussed, but it was argued that the soil-pile model would have to be developed further to account for case-specific phenomena (such as soil heave).

The posterior is not an absolute truth but a reflection of the assumptions the practitioner weaves into the model and applies to construct the priors. Bayesian inference must be applied carefully with an understanding of how decisions in the process including deterministic model assumptions, aleatoric uncertainty assumptions, choice of MCMC algorithm, choice of prior and number of inferred parameters impact the result.

# 6 Code Implementation and Availability

The workflow was implemented in Python on Miniconda. *Scipy* functions *solve_ivp* and *solve_bvp* were used for differential equation solving, and the function *fsolve* was used for simultaneous equation solving. *PyMC* was used for inference. *Arviz* and *Matplotlib* were used for figure generation.

The code and details of the environment are on GitHub at https://github.com/greg-kurzepa/IIBProject.

# 7 Appendix

## 7.1 Analytic DE Solution for Two Soil Layers

For two layers, with pile head boundary condition $F(z = 0) = P$ and pile base boundary condition $F(z = L) = K_b u(z = L)$, the solution can be expressed as eq. 12. The depth of the boundary between the layers is $z_B$. The constants applied to eq. 8 are $B_1$, $C_1$ for the upper layer and $B_2$, $C_2$ for the lower layer.

$$\begin{bmatrix} 1 & -1 & & \\ \exp(\lambda_1 z_B) & \exp(-\lambda_1 z_B) & -\exp(\lambda_2 z_B) & -\exp(-\lambda_2 z_B) \\ \lambda_1 \exp(\lambda_1 z_B) & -\lambda_1 \exp(-\lambda_1 z_B) & -\lambda_2 \exp(\lambda_2 z_B) & \lambda_2 \exp(-\lambda_2 z_B) \\ & & (1+\Omega)(\exp 2L\lambda_2) & \Omega - 1 \end{bmatrix} \begin{bmatrix} B_1 \\ C_1 \\ B_2 \\ C_2 \end{bmatrix} = \begin{bmatrix} -P/AE_P\lambda_1 \\ 0 \\ 0 \\ 0 \end{bmatrix} \tag{12}$$

where

$$\Omega = \frac{K_B}{E_P A \lambda} \tag{13}$$

## 7.2 API Definitions of Ultimate Capacities and Mobilisation Limits

The ultimate shear strength and end bearing strength of the soil in the nonlinear-soil API model are defined as in eq. 14. The effective stress and undrained shear strength profiles are calculated using eq. 15. Additionally, there is a fixed upper limit on the shear and end bearing strength that can be mobilised in sand, expressed in eq. 16.

The end bearing factor $N_q$, shaft friction factor $\beta$, void ratio $e$, dry soil unit weight $\gamma_d$, end bearing mobilisation limit $q_{cap}$ and shaft friction mobilisation limit $\tau_{cap}$ are soil parameters that can be inferred. $z_w$ is the water table depth.

Note that the void ratio parameter $e$ is not physically realistic, since it only impacts the saturated unit weight. In reality, $e$ would be strongly correlated with the other model parameters.

$$\tau = \tau_{ult}\hat{\tau}(u) \qquad \tau_{ult}(z) = \begin{cases} 1.25\beta\sigma'(z) & \text{sand} \\ \alpha s_u(z) & \text{clay} \end{cases}$$

$$\alpha = 1 \qquad \text{underconsolidated clay only} \tag{14}$$

$$Q = Q_{ult}\hat{Q}(u_L) \qquad Q_{ult} = \begin{cases} N_q\sigma'(z) & \text{sand} \\ 9s_u(z) & \text{clay} \end{cases}$$

$$\begin{aligned} \sigma'(z) &= \gamma_d z_w - \frac{1}{1+e}\gamma_w(z - z_w) \\ s_u(z) &= \sigma'(z) \qquad \text{underconsolidated clay only} \end{aligned} \tag{15}$$

$$\begin{aligned} \tau &= \min(\tau_{cap}, \tau) \qquad \text{sand only} \\ Q &= \min(A_{\text{pile}} q_{cap}, Q) \qquad \text{sand only} \end{aligned} \tag{16}$$

## 7.3 Numerical DE Solution Methods and Validation

### 7.3.1 Solver Evaluation

The differential equation solver will be exposed to many different input parameters during sampling so must be robust. Three approaches to solving the differential equation in (link to method) are evaluated. To be accepted as a correct solution, the output displacement profile $u^*(z)$ must fulfill two conditions. Firstly, the boundary condition error (eq. 6) at the top and base of the pile must not exceed 0.1% of the axial pile load. Secondly, the output displacement profile must be consistent with the differential equation at each node. The approaches were assessed for their reliability in fulfilling these conditions.

Before attempting to solve, the algorithms check that the axial load does not exceed the ultimate capacity (in which case a solution does not exist) using eq. 17.

$$P_{ult} = \min(Q_{ult}, Q_{cap}) + \sum_{i=1}^{N} Cdz \min(\tau_{ult}(z_i), \tau_{cap}) \tag{17}$$

**Simultaneous Equations** In this approach, following (21), the pile is split into $N$ elements that are visualised as springs in fig. 13. Each element contains a shear spring connected at a pile spring midpoint to aid numerical accuracy. Elements generate $2N - 1$ simultaneous equations in total, which are solved using *Scipy*'s root-finding *fsolve* function. The simultaneous equations for the linear-elastic pile case is shown in eq. 19.

This method performed poorly; in unpredictable cases negligible changes in the input parameters caused a previously correct solution to fail. Increasing the element count made the solution less reliable. Decreasing the *fsolve* tolerance did not improve reliability.

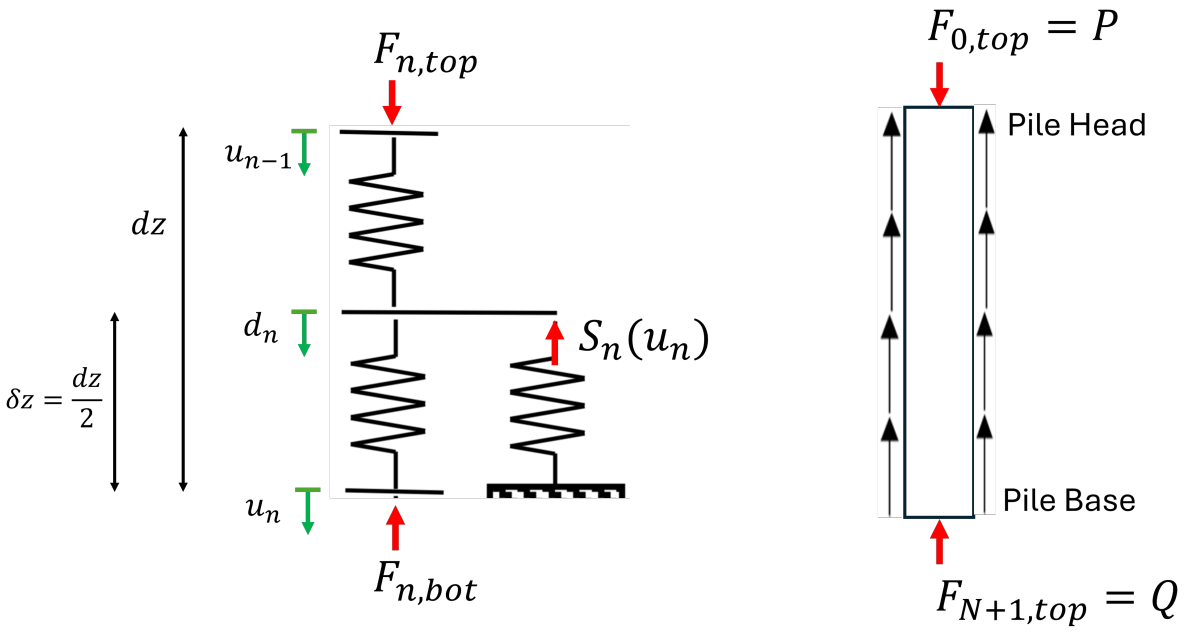


Figure 13: Insert figure caption here

$$
\begin{aligned}
\varepsilon_{n,\text{top}} &= \frac{u_{i-1} - d_i}{\delta z} \\
\varepsilon_{n,\text{bot}} &= \frac{d_i - u_i}{\delta z} \\
S_n &= Cdz \min(\tau_{\text{ult}} \hat{\tau}(d_n), \tau_{cap}) \\
F_{n,\text{top}} &= \begin{cases} -AE_P \varepsilon_{n,\text{top}} & n = 1, \dots N \\ \min(Q_{\text{ult}} \hat{Q}(u_N), Q_{cap}) & n = N+1 \end{cases} \\
F_{n,\text{bot}} &= \begin{cases} P & n = 0 \\ -AE_P \varepsilon_{n,\text{bot}} & n = 1, \dots N \end{cases}
\end{aligned}
\tag{18}
$$

$$
\begin{aligned}
F_{i-1,\text{bot}} - F_{i,\text{top}} &= 0 \quad i = 1, \ldots N+1 \\
F_{i,\text{bot}} + S_i - F_{i,\text{top}} &= 0 \qquad i = 1 \ldots N
\end{aligned}
\tag{19}
$$

**Shooting** In this approach, the strain at the top of the pile is guessed and the differential equation is solved from top to bottom of the pile using Scipy's *solve_ivp* function. The method used by *solve_ivp* here is the "Radau" solver, which is designed to solve stiff nonlinear differential equations. This is a 1-dimensional optimisation problem: selecting the initial strain guess to minimise the equilibrium condition error at the base of the pile. Scipy's *root_scalar* function was used to solve this optimisation problem and thus solve the differential equation.

The method proved to be robust when sufficient discretisation mesh size $N$ and solver tolerance were chosen, as shown in fig. 14. If $N$ was too low or the tolerance was too high, the objective function would be far too jagged for *root_scalar* to solve reliably.

The shooting implementation here was impractically slow to use in inference in SMC in these conditions, where in excess of 10,000 samples may be required per inference.

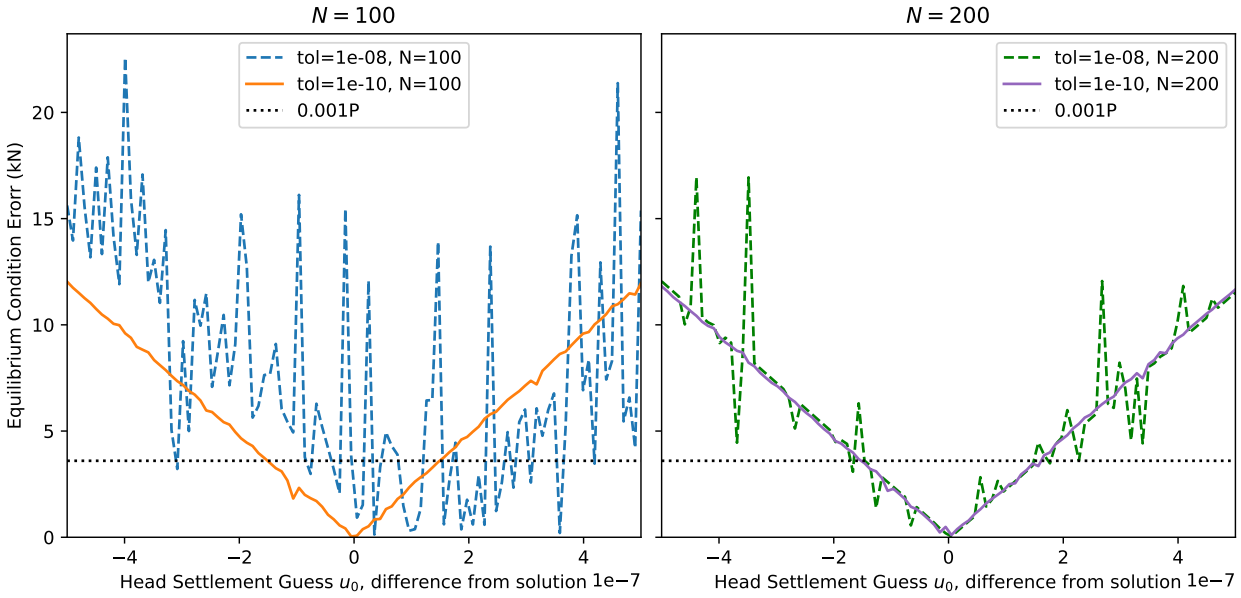


Figure 14: Impact of Scipy *solve_ivp* tolerance and number of pile elements $N$ on the objective function to be minimised (the equilibrium condition at the base of the pile). It it evident that decreasing the tolerance and increasing the element count both improve the smoothness of the objective function. 0.001P is the boundary condition threshold for an acceptable solution.

**Boundary Value Problem** The most successful approach used Scipy's *solve_bvp* function to solve the differential equation. The function iteratively guesses the entire displacement profile until the differential equation and boundary conditions are satisfied. It proved to be robust to a wide range of values and significantly faster than the shooting method, so was the chosen model for inference.

### 7.3.2 Additional Checks

It is known for numerical differential equation solvers based on a Winkler Modulus to struggle when the load is close to the ultimate soil-pile capacity ((19)). The performance of the method at high axial load was tested in fig. 15 and shown to be robust.

To test that the model would work in inference, 1000 samples were taken from the single-variable prior on the dry sand unit weight, as shown in fig. 16. There are no points where the shooting solver did not converge, indicating it is robust for inference with this prior.

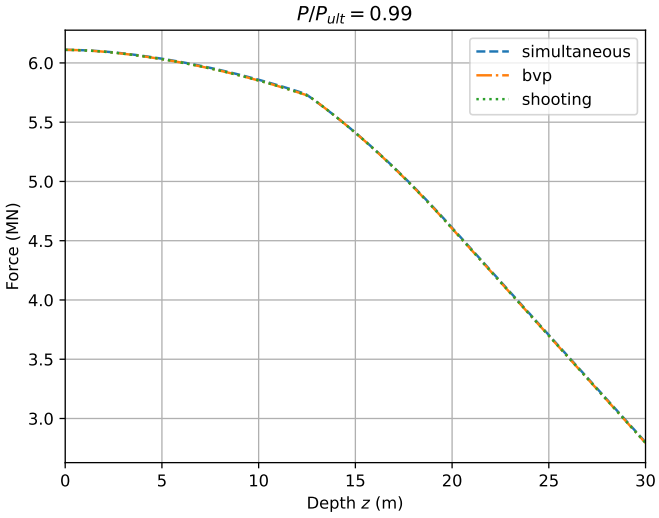


Figure 15:

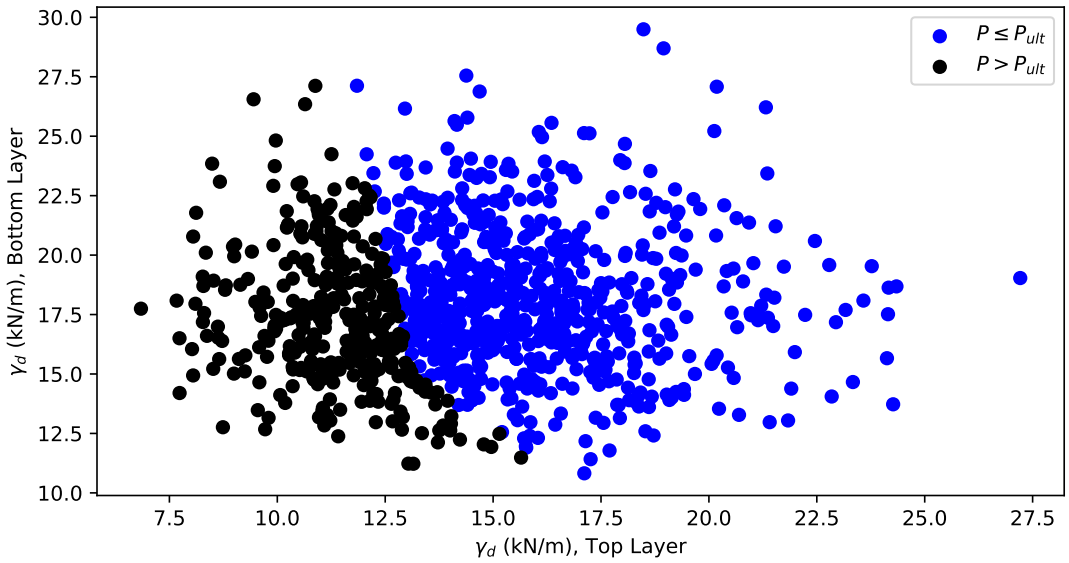


Figure 16: Scatter plot of 1000 samples from the prior on dry soil unit weight for an axial force of 6.1MN, which is close to the ultimate capacity of the pile. The top layer unit weight is along the x-axis and the bottom layer along the y-axis. Points in black indicate where the soil-pile ultimate capacity is exceeded for those unit weights: for these points, the posterior probability of the soil parameter is set to zero since it is physically impossible.

### 7.3.3 Example shaft friction profile

### 7.3.4 Demonstration of Output

An example shaft friction profile generated by the nonlinear API model is shown in fig. 17.

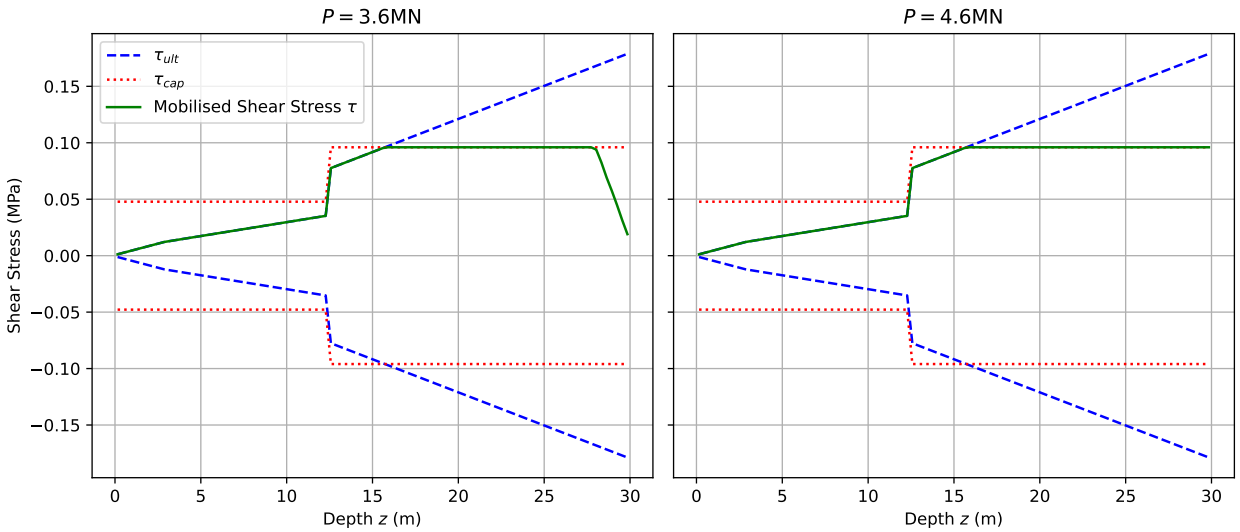


Figure 17: Plot of the mobilised shear stress profile in the soil for the two axial load cases. $\tau_{ult}$ is the ultimate soil strength given the effective stress profile. $\tau_{cap}$ is the API upper limit on soil strength for the sand type. The smallest of these is caps the mobilised shear stress. When the axial load increases to 4.6MN, the overall shear capacity of the soil has been reached and the remainder of the load is taken by the end bearing resistance.

# References

[1] Abril-Pla, O., Andreani, V., Carroll, C., Dong, L., Fonnesbeck, C. J., Kochurov, M., Kumar, R., Lao, J., Luhmann, C. C., Martin, O. A., et al. (2023). Pymc: a modern, and comprehensive probabilistic programming framework in python. *PeerJ Computer Science*, 9:e1516.

[Babanagar] Babanagar, N. BIM INTEGRATION OF MONITORING DATA FOR BASEMENT CONSTRUCTION.

[3] Baecher, G. B. (2023). 2021 Terzaghi Lecture: Geotechnical Systems, Uncertainty, and Risk. *Journal of Geotechnical and Geoenvironmental Engineering*, 149(3):03023001.

[4] Bateman, A. H., Crispin, J. J., Vardanega, P. J., and Mylonakis, G. E. (2022). Theoretical t-z Curves for Axially Loaded Piles. *Journal of Geotechnical and Geoenvironmental Engineering*, 148(7):04022052.

[5] Buckley, R., Chen, Y. M., Sheil, B., Suryasentana, S., Xu, D., Doherty, J., and Randolph, M. (2023). Bayesian Optimization for CPT-Based Prediction of Impact Pile Drivability. *Journal of Geotechnical and Geoenvironmental Engineering*, 149(11).

[6] Burke, T. D. S., Jacobsz, S., Elshafie, M., and Osman, A. (2022). Measurement of pile uplift forces due to soil heave in expansive clays. *Canadian Geotechnical Journal*, 59(12):2119–2134.

[7] Cañavate-Grimal, A. and Nicholson, D. (2021). A probabilistic analysis to assess the most probable design parameters for use in the observational method.

[8] Chai, X., Rózsás, Á., Slobbe, A., and Teixeira, A. (2022). Probabilistic parameter estimation and reliability assessment of a simulated sheet pile wall system. *Computers and Geotechnics*, 142:104567.

[9] Christian, J. T. (2004). Geotechnical Engineering Reliability: How Well Do We Know What We Are Doing? *Journal of Geotechnical and Geoenvironmental Engineering*, 130(10):985–1003.

[10] Christian, J. T. and Baecher, G. B. (2011). Unresolved Problems in Geotechnical Risk and Reliability. In *GeoRisk 2011*, pages 50–63, Atlanta, Georgia, United States. American Society of Civil Engineers.

[11] Huang, M., Ninić, J., and Zhang, Q. (2021). Bim, machine learning and computer vision techniques in underground construction: Current status and future perspectives. *Tunnelling and Underground Space Technology*, 108:103677.

[12] Institute, A. P. (2021). Geotechnical and foundation design considerations.

[13] Juang, C. H. and Zhang, J. (2017). Bayesian Methods for Geotechnical Applications—A Practical Guide. In *Geotechnical Safety and Reliability*, pages 215–246, Denver, Colorado. American Society of Civil Engineers.

[14] Luo, L., Mei, Y., Battista, N., Kechavarzi, C., and Soga, K. (2021). Repeatability precision

error analysis of the distributed fiber optic strain monitoring. *Structural Control and Health Monitoring*, 28(8).

[15] McNeish, D. (2016). On Using Bayesian Methods to Address Small Sample Problems. *Structural Equation Modeling: A Multidisciplinary Journal*, 23(5):750–773.

[16] Park, J. H., Kim, D., and Chung, C. K. (2012). Implementation of Bayesian theory on LRFD of axially loaded driven piles. *Computers and Geotechnics*, 42:73–80.

[17] Phoon, K.-K., Cao, Z.-J., Ji, J., Leung, Y. F., Najjar, S., Shuku, T., Tang, C., Yin, Z.-Y., Ikumasa, Y., and Ching, J. (2022). Geotechnical uncertainty, modeling, and decision making. *Soils and Foundations*, 62(5):101189.

[Poulos] Poulos, H. G. Pile behaviour—theory and application.

[19] Psaroudakis, E. G., Mylonakis, G. E., and Klimis, N. S. (2019). Non-Linear Analysis of Axially Loaded Piles Using "t–z" and "q–z" Curves. *Geotechnical and Geological Engineering*, 37(4):2293–2302.

[20] Quigley, P., Buggy, F., Clancy, J., Condron, M., Finnerty, C., Gill, D., Hayes, G., Luby, D., and Ryan, M. (2016). Some trends from recent geotechnical projects in Ireland. *Proceedings of the Institution of Civil Engineers - Forensic Engineering*, 169(3):83–93.

[21] Rocscience (2022). Axially loaded piles theory.

[22] Shahin, M. A. (2016). State-of-the-art review of some artificial intelligence applications in pile foundations. *Geoscience Frontiers*, 7(1):33–44.

[23] Sheil, B. B., Suryasentana, S. K., Templeman, J. O., Phillips, B. M., Cheng, W.-C., and Zhang, L. (2022). Prediction of Pipe-Jacking Forces Using a Bayesian Updating Approach. *Journal of Geotechnical and Geoenvironmental Engineering*, 148(1).

[24] Van De Schoot, R., Depaoli, S., King, R., Kramer, B., Märtens, K., Tadesse, M. G., Vannucci, M., Gelman, A., Veen, D., Willemsen, J., and Yau, C. (2021). Bayesian statistics and modelling. *Nature Reviews Methods Primers*, 1(1):1.

[25] Wang, Y., Cao, Z., and Li, D. (2016). Bayesian perspective on geotechnical variability and site characterization. *Engineering Geology*, 203:117–125.

[26] Yeow, H.-C., Nicholson, D., Man, C.-L., Ringer, A., Glass, P., and Black, M. (2014). Application of observational method at Crossrail Tottenham Court Road station, UK. *Proceedings of the Institution of Civil Engineers - Geotechnical Engineering*, 167(2):182–193.